ADVANCED ELECTRONIC MATERIALS
www.advelectronicmat.de

Nonvolatile Electric-Field Control of Ferromagnetic Resonance and Spin Pumping in Pt/YIG at Room Temperature

Rui Yu, Kang He, Qi Liu, Xucheng Gan, Bingfeng Miao, Liang Sun, Jun Du, Hongling Cai, Xiaoshan Wu, Mingzhong Wu, and Haifeng Ding**

Electric-field-controlled magnetism is of importance in realizing energy efficient, dense and fast information storage and processing. Strain-mediated converse magneto-electric (ME) coupling between ferromagnetic and ferroelectric heterostructure shows promise for realizing electric-controlled magnetism at room temperature and is attracting a number of recent investigations. However, such ME-effect studies have mainly focus on magnetic metals. In this work, high quality yttrium iron garnet ($Y_3Fe_5O_{12}$ (YIG)) films are deposited directly onto (100)-oriented single-crystal Pb $(Mg_{1/3}Nb_{2/3})_{0.7}Ti_{0.3}O_3$ (PMN-PT) substrates by means of magnetron sputtering. The electric-field-induced polarization switching and lattice strain in the PMN-PT substrate results in two distinct magnetization states in the YIG film that are nonvolatile and electrically reversible. Because of the direct contact between the YIG and the PMN-PT substrate, an efficient ME coupling and an almost 90° rotation of the easy axis of the YIG film can be realized. Furthermore, the electric-field-controlled hysteresis loop-like ferromagnetic resonance field shifts and spin pumping signals are observed in Pt/YIG/PMN-PT heterostructures. Thus, the obstacle is overcome via growing high-quality YIG thin films directly onto PMN-PT substrates and an efficient manipulation of magnetism and pure spin current transport by electric field is thereby realized. These findings are instructive for future low-power magnetic insulator-based spintronic devices.

Electric-field-controlled magnetism is crucial to realize energy efficient, dense, and fast information storage and processing.[1–3] The converse magnetoelectric (ME) coupling permits the manipulation of magnetism by electric field instead of magnetic field or electric current. Thus, multiferroic materials that couple ferromagnetic and ferroelectric order have drawn considerable interest. Room temperature, single-phase multiferroic materials, however, are still rare, and the converse ME effects are typically small.[4,5] Strain-mediated ME coupling between ferromagnetic (FM) and ferroelectric (FE) heterostructures that serve as an alternative approach to realize electric-field controlled magnetism at room temperature have been intensively investigated recently.[6–8] In these materials, the electric-field induced piezostrain in the FE layer induces an effective magnetic anisotropy in FM layer.[9–11] Converse ME effect studies usually focus on magnetic metals. For instance, Zhang et al. reported the nonvolatile tuning of magnetization in $Co_{40}Fe_{40}B_{20}$/Pb $(Mg_{1/3}Nb_{2/3})_{0.7}Ti_{0.3}O_3$ (PMN-PT) structures,[12] while Liu et al. reported the nonvolatile tuning of ferromagnetic resonance (FMR) of the magnetically soft CoFeB alloy using ferroelectric domain switching of PMN-PT substrates.[13] Meanwhile, increasing attention has focused on magnetic insulators, where a pure spin current can transport with no accompanying charge carriers.[14] With the absence of Joule heating, magnetic insulators have great potential in ultralow power information technologies.[15,16] Experimentally, magnon-based logic gates and transistors have been realized.[17–19] Among various magnetic insulators, yttrium iron garnet ($Y_3Fe_5O_{12}$ (YIG)), has attracted considerable attention due to its large bandgap, ultralow damping, weak anisotropy, and high Curie temperature.[20,21] In addition to its indispensable contribution to microwave devices, YIG has experienced a resurgence of interest from the spintronics community. YIG provides a perfect platform for pure spin current related study, including spin pumping,[22–24] spin Seebeck effect,[25,26] and spin torque oscillators,[27] due to its low loss and long diffusion length for spin currents.[21] However, high quality YIG thin films generally can only be obtained on gallium gadolinium garnet (GGG) substrates, to which it has a closely matched lattice constant.[28] YIG film growth on FE substrates is still rare due to the large lattice mismatch and high annealing temperature required for YIG film crystallization. Thus, in YIG-based

R. Yu, K. He, Q. Liu, X. Gan, Prof. B. Miao, Prof. L. Sun, Prof. J. Du, Prof. H. Cai, Prof. X. Wu, Prof. H. Ding
National Laboratory of Solid State Microstructures
and Department of Physics
Nanjing University
22 Hankou Road, Nanjing 210093, P. R. China
E-mail: bfmiao@nju.edu.cn; hfding@nju.edu.cn

R. Yu, Prof. M. Wu
Department of Physics
Colorado State University
Fort Collins, CO 80523, USA

Prof. B. Miao, Prof. L. Sun, Prof. J. Du, Prof. H. Cai, Prof. X. Wu, Prof. H. Ding
Collaborative Innovation Center of Advanced Microstructures
Nanjing University
22 Hankou Road, Nanjing 210093, P. R. China

The ORCID identification number(s) for the author(s) of this article can be found under https://doi.org/10.1002/aelm.201800663.

DOI: 10.1002/aelm.201800663

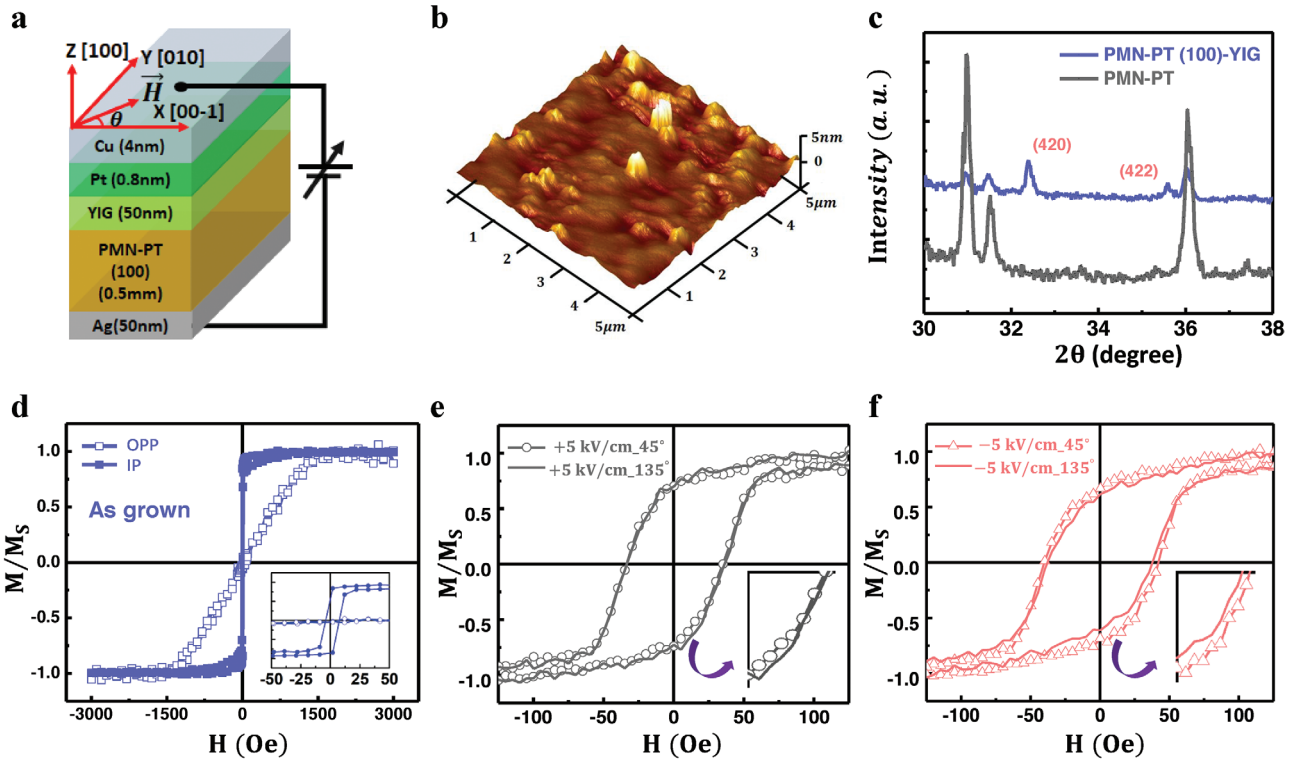

Figure 1. a) Schematic illustration of the experimental setup to realize electric-field-controlled magnetism of YIG. b) The AFM image of YIG film after annealing. c) XRD $\theta - 2\theta$ scan of the PMN-PT (100) substrate (black) and annealed YIG films deposited on a PMN-PT substrate (blue). The curves have been shifted for clarity. d) *M–H* loop of as-grown YIG/PMN-PT (100) heterostructure along the vertical (open squares) and in-plane direction (solid squares). The inset presents the *M–H* loop near zero field. e,f) In-plane *M–H* loops of YIG/PMN-PT heterostructure measured with magnetic field along $\theta = 45°$ and 135° under electric field of +5 and −5 kV cm^{-1}, respectively. The inset of (d–f) presents the zoomed-in feature near zero field.

multiferroic heterostructures, epoxy is frequently used to bond YIG onto the FE substrates. This type of bonding, however, strongly reduces the ME interaction and only a limited FMR tuning range was reported in the YIG-lead zirconate titanate (PZT) and YIG-Y-cut langatate (LGT) systems.[29,30] Therefore, it is desirable to deposit YIG onto FE substrates directly to achieve efficient and nonvolatile electric-field-controlled tuning of the magnetism.

In this work, we deposited high quality YIG films directly onto (100)-oriented single-crystal PMN-PT substrates by means of magnetron sputtering. Our YIG films exhibit a negligible in-plane anisotropy with a coercivity of ≈5 Oe, which is comparable with those grown on GGG substrates.[28] The electric-field-induced polarization switching and lattice strain in the PMN-PT substrate results in two distinct magnetization states in the YIG film that are nonvolatile and electrically reversible. Because of the direct contact between the YIG and the PMN-PT substrate, we can realize an efficient ME coupling and an almost 90° rotation of the easy axis of the YIG film. Furthermore, the electric-field-controlled hysteresis loop-like FMR resonance field shifts and spin pumping signals are observed in Pt/YIG/PMN-PT heterostructures. We, thus, overcame the obstacle via growing high-quality YIG thin films directly onto PMN-PT substrates and thereby realized an efficient manipulation of magnetism and pure spin current transport by electric field. These findings are instructive for future low-power magnetic insulator-based spintronic devices.

0.5 mm thick single-crystal PMN-PT (100) is chosen as the substrate because it exhibits strong piezoelectric behavior. The sample edges (*x*, *y*, and *z*) were cut along the pseudocubic [00-1], [010], and [100] direction of the PMN-PT, as shown in **Figure 1**a. A 50 nm thick YIG film was deposited onto the PMN-PT (100) substrate by RF magnetron sputtering at room temperature. The film was further annealed at 800 °C in air for 4 h. The YIG film has a smooth surface with an rms roughness of only ≈0.3 nm, as revealed by atomic force microscopy (AFM) (see Figure 1b). Figure 1c presents the X-ray diffraction (XRD) θ-2θ scan of the PMN-PT substrate and the YIG (50 nm)/PMN-PT sample. The additional two peaks in the latter are from the (420) and (422) peaks of YIG, indicating the polycrystalline nature of the YIG film. The magnetic properties of the YIG/PMN-PT heterostructure (as-grown) are investigated using vibrating sample magnetometer (VSM). The hysteresis loop of the as-grown YIG film under an in-plane magnetic field is almost square, while the loop with an out-of-plane magnetic field shows a hard axis behavior, as shown in Figure 1d. The inset presents the *M–H* loop near zero field. The small coercivity of H_c = 5.4 Oe indicates a weak in-plane anisotropy in our samples and permits low magnetic loss.[20] These results are comparable with those of YIG films deposited on GGG substrates.[28]

In order to investigate the electric-field-controlled properties of the YIG/PMN-PT FM/FE heterostructures, a 50 nm thick Ag layer was grown as the bottom electrode using DC magnetron

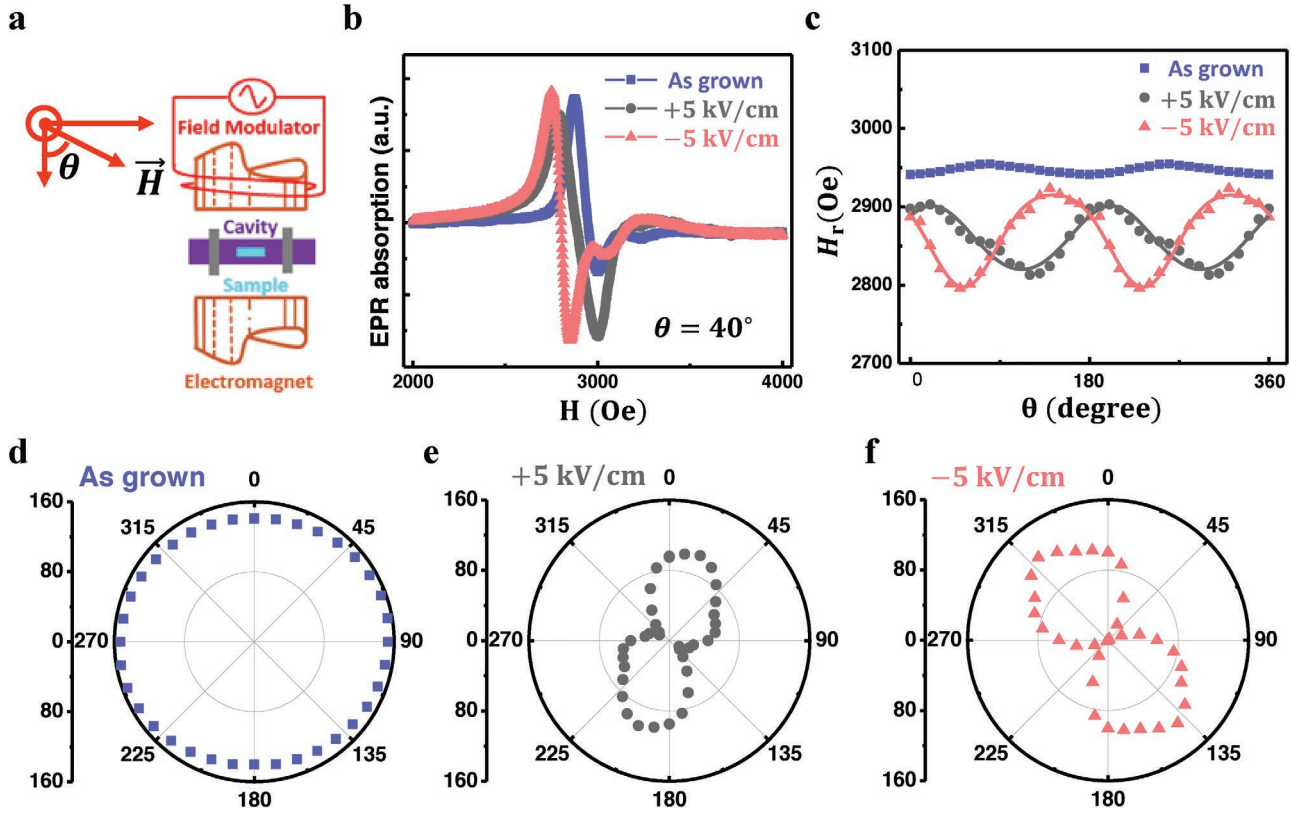

Figure 2. a) Schematic illustration of the experimental setup for FMR spectrum measurements. b) Typical FMR spectra of the as-grown YIG and after applying with electric fields of ±5 kV cm^{-1} at $\theta = 40°$ under the microwave excitation at 9.78 GHz. c) Angular dependent resonance field for the as-grown YIG film and with an applied field of ±5 kV cm^{-1}. Symbols are the experimental data and the lines are fitting results by using Equation (1). d–f) Replots of c) in the polar map upon different conditions. Note that a background of 2800 Oe is subtracted for better illustration.

sputtering. A Pt (0.8 nm)/Cu (4 nm) layer was grown on top of the structure and served as the top electrode as well as the pure spin current detecting layer and the protective layer. A schematic diagram of the sample sequence and the experimental configuration is shown in Figure 1a. The electric field is applied along the z-direction, with the gate voltage V defined as the voltage at the top electrode with respect to the bottom one. We note that before the electric field dependent measurements, five cycles sweeping of electric field between −5 and +5 kV cm^{-1} were performed to reduce the memory effect. All curves were obtained after the removal of the electric field. We performed the XRD measurements after polarizing the film with ±5 kV cm^{-1} and did not observe apparent shift of the XRD peak (<0.03%). This could be understood as the typical in-plane strain of PMN-PT is only ≈0.1% under 5 kV cm^{-1}.[12,31,32] With the relatively large thickness (50 nm) of the YIG film, the strain should be significantly smaller. Figure 1e presents M–H loops of YIG after applying +5 kV cm^{-1}, where the magnetic fields were aligned along $\theta = 45°$ (open squares) and 135° (solid square). In both cases, the coercivity value increases to ≈32 Oe due to the piezostrain induced by the PMN-PT. Interestingly, the magnetization value at low field for $\theta = 45°$ is smaller than that for $\theta = 135°$ (see the amplified view in the inset), indicating that the direction of the easy axis is closer to $\theta \approx 135°$ for +5 kV cm^{-1}. Similar measurements were carried out after applying an electric field of −5 kV cm^{-1}; the results (Figure 1f) show the opposite behavior compared to those obtained for +5 kV cm^{-1}. Namely, the magnetization value at low field for $\theta = 45°$ (open circles) is larger than that for $\theta = 135°$ (solid line), as shown in the amplified view in the inset. These results demonstrate that the electric field can induce an effective modulation on the magnetic anisotropy of the YIG film.

To obtain quantitative information on the modulation of the magnetic anisotropy of our samples, angle-dependent FMR measurements were carried out, with the schematic illustration of the experimental setup shown in **Figure 2**a. Figure 2b presents typical FMR spectra of the as-grown YIG and the film with an electric field of ±5 kV cm^{-1} applied for $\theta = 40°$. Note that the as-grown film refers to the sample where the top and bottom electrodes have not been grown and for which no electric-field sweeping was carried out. Under microwave excitation at 9.78 GHz, FMR occurs at H_r = 2946 Oe for the as-grown YIG film. After the electric field is applied, the resonance fields shift to lower values due to the strain-induced anisotropy. The H_r value for the YIG/PMN-PT heterostructure after applying +5 kV cm^{-1} (−5 kV cm^{-1}) is larger (smaller), exhibiting a hard (easy) axis behavior, consistent with the hysteresis loop measurements in Figures 1e,f (45°case). In order to quantify the anisotropy constants, angular dependent FMR measurements were performed; the data are presented in Figure 2c. The relation between the resonance field H_r and the microwave frequency f is determined by the equation[33]

$$f = \frac{\gamma}{2\pi}\sqrt{\left\{H_r + H_{4\parallel}\cos 4\left(\phi-\phi_u\right) + H_{2\parallel}\cos 2\left(\phi-\phi_u\right)\right\}\left\{H_r + 4\pi M_{\text{eff}} + \frac{H_{4\parallel}}{4}\left[3+\cos 4\left(\phi-\phi_u\right)\right] + \frac{H_{2\parallel}}{2}\left[1+\cos 2\left(\phi-\phi_u\right)\right]\right\}} \quad (1)$$

where $\frac{\gamma}{2\pi}$ is the gyromagnetic ratio ≈2.8 GHz/kOe, $H_{2\parallel}$ is the in-plane uniaxial anisotropy field, $H_{4\parallel}$ is the in-plane four-fold anisotropy field, M_{eff} is the effective magnetization, ϕ denotes the angle between magnetization and *x*-axis, and ϕ_u denotes the angle between one of the in-plane uniaxial anisotropy axes and *x*-axis. For the as-grown YIG film (blue circle), H_r is almost constant when rotating the in-plane field. Fitting the H_r–θ curve with Equation (1), we determine the in-plane uniaxial anisotropy field $H_{2\parallel}$ = 7.7 Oe, and the in-plane fourfold anisotropy field $H_{4\parallel}$ = 0.5 Oe, respectively. After polarizing the PMN-PT substrate, we observed a >100 Oe modulation of H_r of the YIG film for the 9.78 GHz excitation, which is more than one order of magnitude larger than the modulation of ≈6 Oe for the 5-GHz excitation[29] where the YIG film was not directly bonded onto the FE substrate. Fitting the angular dependent H_r curves, we obtain $H_{2\parallel}$ = 50.8 Oe and $H_{4\parallel}$ = 2.6 Oe for YIG/PMN-PT under +5 kV cm^{-1}, and $H_{2\parallel}$ = –74.0 Oe and $H_{4\parallel}$ = –12.9 Oe for YIG/PMN-PT under –5 kV cm^{-1}. In consistent with the clear two-fold symmetries observed in Figure. 2c, we find $H_{2\parallel}$ is much larger than $H_{4\parallel}$ for all three cases. And $H_{2\parallel}$ of YIG/PMN-PT is considerably larger after the application of the electric field. When the YIG/PMN-PT is positively (negatively) polarized, the easy axis lies along 120°/300° (50°/230°). To better illustrate the effect, we also present the corresponding H_r–θ plots in the polar maps in Figure 2e,f), which demonstrate the influence of the electric field on the magnetic anisotropy of the YIG film. The resonance field H_r curve of the as-grown YIG film is almost a circle, indicating negligible in-plane magnetic anisotropy. After being electrically polarized, a sizable uniaxial magnetic anisotropy emerges, where the easy axis depends on the direction of the applied electric field. Compared with the as-grown YIG film, the easy axis for the positively (negatively) polarized case shifts about 60° (50°) counterclockwise (clockwise). Thus, we demonstrated the direct deposition of YIG films onto PMN-PT with similar magnetic properties as for YIG films grown on GGG substrates, and we observed a close to 90° rotation of the magnetic anisotropy axis for the YIG/PMN-PT heterostructure.

In addition to applications in microwave devices, YIG is also widely used as a pure spin current source for spintronics studies, including studies on the spin pumping[22–24] and the spin Seebeck effect.[25,26] Here spin pumping refers to the injection of a pure spin current by a YIG film into a neighboring nonmagnetic material during FMR with microwave excitation.[34] YIG is also used to quantify the spin Hall angle of nonmagnetic metals with strong spin-orbit coupling due to its favorable interface and being free from an impedance mismatch.[34] **Figure 3**a presents a schematic illustration of the experiment setup for electric-field-controlled spin pumping. The sample is placed onto a coplanar waveguide. In order to achieve high sensitivity, we modulate the microwave with TTL out signal from a lock-in amplifier, which further picks up the voltage signal as a function of external magnetic field. Under microwave excitation, the magnetization of the YIG film precesses and pumps the spin current $\vec{j}_s$ into the Cu (4 nm)/Pt (0.8 nm). $\vec{j}_s$ is further converted into an electrically detectable charge current $\vec{j}_c$ via the inverse spin Hall effect (ISHE) through $\vec{j}_c = (2e/\hbar)\theta_{SH}\vec{j}_s \times \vec{\sigma}$, where $\vec{\sigma}$ denotes the spin-polarization direction of $\vec{j}_s$ and is parallel to the magnetic field, and $\hbar$ is the reduced Planck constant, θ_{SH} is the spin Hall angle.[35] The spin pumping voltage can be described by

$$V_{SP} = J_s(0)\frac{2e}{\hbar}Rw\lambda_{sd}\theta_{SH}\tanh\left(\frac{t_{Pt}}{2\lambda_{sd}}\right) \quad (2)$$

where λ_{sd}, *R*, and *w* is the spin diffusion length of Pt, resistance (980 Ω), and width (0.5 mm) of Cu/Pt stripe, respectively. And $J_S(0)$ refers to the spin current that pumped into Pt at the interface. Figure 3b presents typical curves for as-grown Cu (4 nm)/Pt (0.8 nm)/YIG/PMN-PT measured at 6 GHz. A positive spin-pumping-induced voltage V_{SP} is obtained, exhibiting a symmetrical Lorentzian shape with the resonance field at 1516 Oe when the magnetic field is along the *x*-axis (+*H*).[36,37] Reversing the field direction changes the sign of the voltage but not its magnitude, which provides evidence of its pure spin current origin. We performed similar measurements of spin pumping at different microwave frequencies and obtained a relationship between *f* and H_r that fits the Kittel Equation (Figure 3c). The result yields a saturation induction of $4\pi M_{\text{eff}}$ = 1377 Oe, which is comparable to the reported values of YIG film grown by magnetron sputtering.[38] The inset of Figure 3c presents the linear dependence of half linewidth Δ*H* of Cu (4 nm)/Pt (0.8 nm)/YIG/PMN-PT (as-grown)on PMN-PT on microwave frequency. From $\Delta H = \Delta H_0 + \alpha f\frac{2\pi}{\gamma}$ we obtain the damping factor $\alpha = (8.55 \pm 0.48) \times 10^{-3}$, which is comparable with the reported values for polycrystalline YIG thin film.[39,40]

Since spin pumping is closely related to the dynamics of the ferromagnet,[41] it is also interesting to study the influence of the electric field on it. Figures 3d–i present the spin pumping signal V_{SP} after being polarized under different electric field values (from +5 to –5 kV cm^{-1} and back to +5 kV cm^{-1}), where the magnetic field is along the *x*-axis and *f* = 6 GHz. At +5 kV cm^{-1} polarization, the resonance field H_r is ≈1522 Oe and the amplitude of V_{SP} is ≈0.85 μV (Figure 3d). Decreasing the electric-field to –0.5 kV cm^{-1} does not introduce any apparent changes (Figure 3e). However, a noticeable decrease of the H_r values to ≈1472 Oe is observed upon further decreasing the electric field to –4 kV cm^{-1} (Figure 3f). Meanwhile, V_{SP} also decreases to ≈0.77 μV. We obtain a similar curve when the sample has been negatively polarized at –5 kV cm^{-1} (Figure 3g). Increasing the electric field back to +5 kV cm^{-1} gives the reverse behavior. The signal does not change significantly when the electric field is increased back to +0.5 kV cm^{-1} (Figure 3h). However, a sharp change occurs after the electric field is further increased to +4 kV cm^{-1} with H_r = 1522 Oe and V_{SP} = 0.85 μV, which are almost the same values as for the initial stage with +5 kV cm^{-1} (Figure 3i). Thus, we observed a two-level control of both H_r and V_{SP} within one cycle of electric-field modulation. This demonstrates that the electric field does not only influence the anisotropy constant, but also modulates the spin pumping

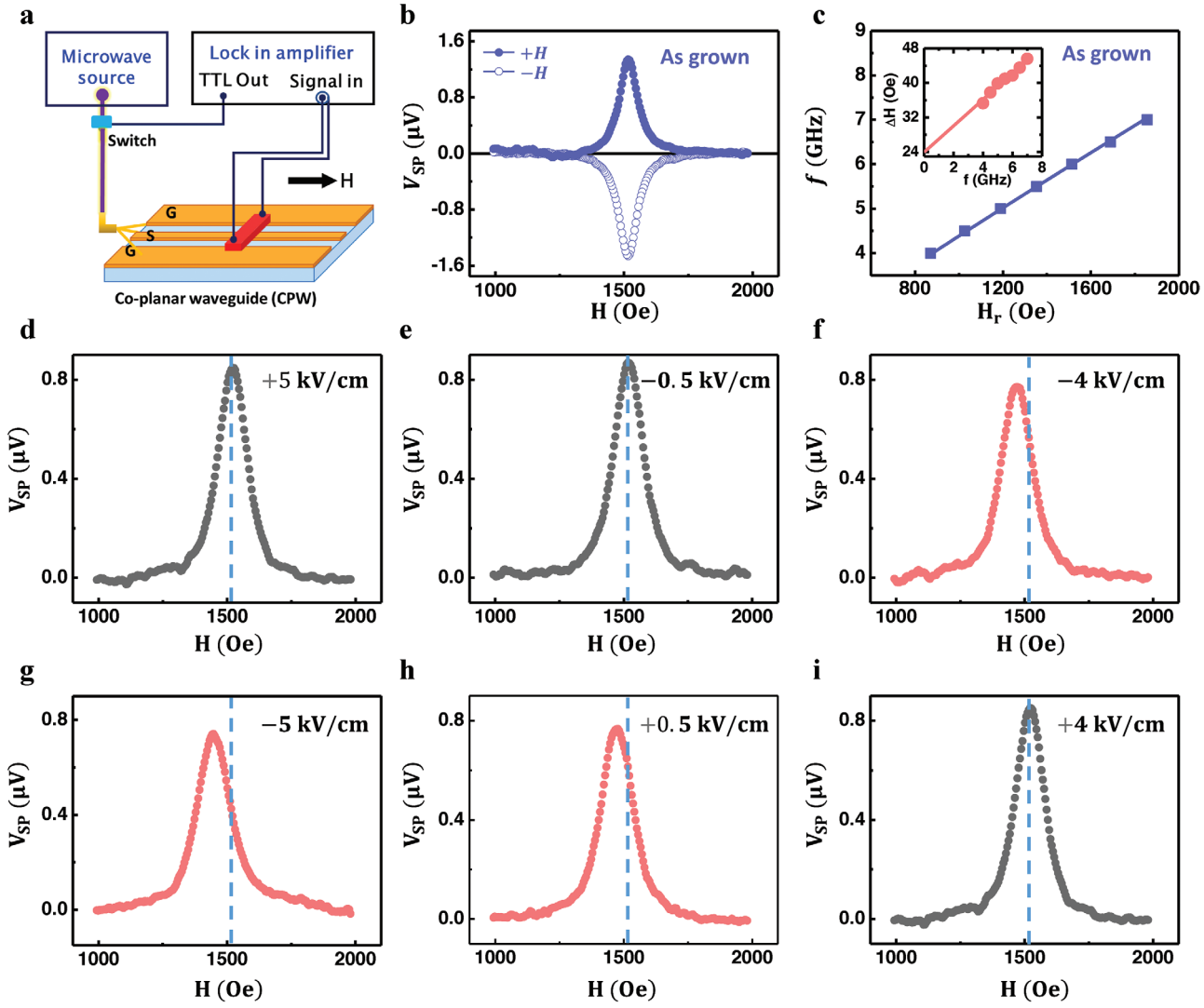

Figure 3. a) Schematic illustration of the experimental setup to perform the electric-field-controlled spin pumping experiments. b) Typical curves of the spin pumping signal for Cu (4 nm)/Pt (0.8 nm)/YIG/PMN-PT (as-grown) measured at 6 GHz along +*x*-direction (+*H*) and –*x*-direction (–*H*). c) The microwave frequency *f* dependent resonance field H_r. Symbols are the experimental data and the line is the fitting using Kittel's Equation. Inset presents the linear dependence of half linewidth of Cu (4 nm)/Pt (0.8 nm)/YIG/PMN-PT (as-grown) on *f*. Symbols are the experimental data and the line is the linear fitting. d–i) Snapshots of the spin pumping signal V_{SP} after being polarized with different electric fields (from +5 to −5 kV cm^{-1}, and back to +5 kV cm^{-1}), where the magnetic field is along the *x*-axis. The vertical lines corresponding to the resonance field of as-grown YIG and are used to illustrate the relative peak shift.

signal of the Cu (4 nm)/Pt (0.8 nm)/YIG/PMN-PT.[42,43] We note that all the spin pumping measurements were performed in the absence of an electric field. Thus, the electric-field-controlled behavior of both the resonance field and the spin pumping are nonvolatile.

Figures 4a,b summarize the electric-field-dependent resonance field H_r and spin pumping amplitude V_{SP} (H_r) (the spin pumping voltage obtained at H_r). Both quantities exhibit hysteresis loop features as we sweep the electric field. H_r and V_{SP} are larger (smaller) when the PMN-PT substrate is positively (negatively) polarized, and the switches occur at around ±3 kV cm^{-1}. The loop-like electric responses of H_r and V_{SP} are associated with the polarization switching of the PMN-PT substrate, as revealed by the polarization current peak shown in Figure 4c and the ferroelectric hysteresis loop shown in Figure 4c inset. Otherwise, butterfly-type curves would be obtained if only polarization rotation is involved. Along with the electric-field controlled spin pumping voltage, we also find the simultaneous change of half linewidth of FMR curves. The spin pumping voltage is larger when ΔH is smaller, as presented in Figure 4d. This could be partially understood as follows. The narrower FMR line leads to the increased angle of precession, resulting in the increased V_{SP}. Therefore, we observe an inverse relationship between the FMR linewidth and V_{SP}. Similar observations have also been reported in other systems.[42,44] The observed inversed relation also indicates the modulation of the spin pumping voltage is caused by the change of the spin pumping efficiency. Due to the large thickness of YIG and small thickness of Pt, we

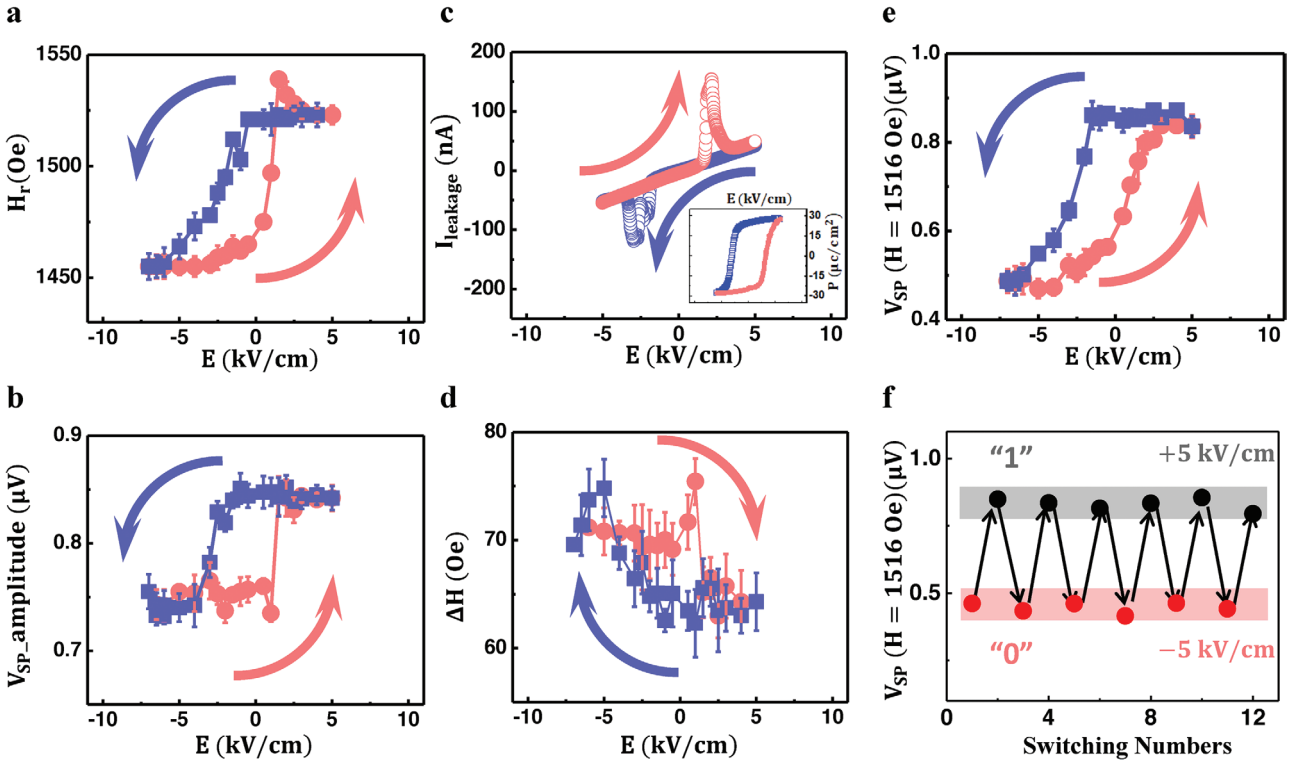

Figure 4. Electric field-dependent a) resonance field H_r and b) spin pumping amplitude V_{SP} (H_r) for Cu (4 nm)/Pt (0.8 nm)/YIG/PMN-PT. c) Polarization current loop of PMN-PT and ferroelectric hysteresis loop of PMN-PT (inset). Electric-field-dependent d) half linewidth and e) spin pumping signal for Cu (4 nm)/Pt (0.8 nm)/YIG/PMN-PT obtained at 1516 Oe (the resonance field of the as-grown YIG). f) Electric-field-induced, nonvolatile switching of the spin pumping signal under a fixed magnetic field of 1516 Oe.

find the damping factors of YIG and YIG capped with Cu/Pt are almost the same within experimental error margin. Thus, we did not obtain a meaningful effective mixing conductance of Pt-YIG interface. Using the reported spin Hall angle (0.032) and spin diffusion length (8.4 nm) of Pt,[34] we estimated the injected spin current density with Equation (2) and found it varied from 4.4×10^{-11} J m^{-2} (+5 kV cm^{-1}) to 3.9×10^{-11} J m^{-2} (−5 kV cm^{-1}). The estimated spin current density is comparable with previous reported values for Pt on single-crystalline YIG substrate (10^{-11}–10^{-9} J m^{-2}).[45]

We emphasize that in the hysteresis loop of the spin pumping amplitude V_{SP} (H_r), the magnetic field is not a constant for different electric fields, as the electric field also has influence on the anisotropy constant, as on the resonance field H_r. Although one can find two levels for the spin pumping voltage amplitude V_{SP} (H_r), it would be more appealing to realize the two-level states with electric-field modulation only. Interestingly, if the magnetic field is fixed at the resonance field of the as-grown YIG/PMN-PT system, $H_0 = 1516$ Oe, the spin pumping voltage V_{SP} ($H = H_0$) also has a loop-like response with the electric field, as presented in Figure 4e. As the PMN-PT is subjected to +5 kV cm^{-1}, the remnant state "1" results in a maximum value (Figure 4f); Upon applying −5 kV cm^{-1} electric-field, the spin pumping voltage switches to the remnant state "0" with a minimum value (Figure 4f); further reversing the electric field back to +5 kV cm^{-1} returns the pumping voltage to its maximum value (Figure 4f). Such a procedure can be repeated without any apparent attenuation. Therefore, nonvolatile, tunable, and stable high/low voltage states can be achieved by switching the polarity of the electric field only.

In summary, we have grown high-quality YIG thin films directly onto single-crystal ferroelectric PMN-PT substrates by magnetron sputtering. Due to the efficient direct coupling at the interface between the YIG and the PMN-PT, considerable FMR frequency modulation and an almost 90° rotation of the anisotropy easy axis of YIG by ferroelectric polarization switching only were demonstrated. Both the FMR resonance field and the spin pumping amplitude exhibit hysteresis-loop behavior when sweeping the applied electric field. Furthermore, two distinct, stable, and nonvolatile states were realized by switching the polarity of the electric field only. These achievements may pave a way for applications of insulator-based FM/FE heterostructures and attract more interest in electric-field-controlled magnetism in magnetic insulators, which already play increasingly important roles in spintronic devices.

Experimental Section

A 50 nm thick YIG film was deposited onto a (100) PMN-PT substrate by RF magnetron sputtering at room temperature in an Ar pressure of 0.3 Pa and a target-to-substrate distance of 6.9 cm. The film was annealed at 800 °C for 4 h in air. The morphology and structural properties of the YIG film were characterized by AFM and XRD, respectively. The capping bilayer Pt (0.8 nm)/Cu (4 nm) and the bottom electrode Ag (50 nm) were deposited using DC magnetron sputtering at room temperature. The magnetic hysteresis loops were measured using a

VSM at room temperature. The ferromagnetic resonance spectra were measured using a commercial electron paramagnetic resonance (EPR) apparatus as well as a homemade spin pumping setup. For the same sample, both techniques yielded the same linewidth. The spin pumping signal was obtained using our home-designed coplanar waveguide. The leakage current for PMN-PT substrate under sweeping electric field was measured on Keithley 6517B. The ferroelectric hysteresis loops were measured on a Precision Premier II (Radiant Technologies, Inc.). All experiments were performed at room temperature.

Acknowledgements

Work at NJU was supported by the National Key R&D Program of China (Grant No. 2018YFA0306004 and 2017YFA0303202), the National Natural Science Foundation of China (Grants No. 51601087, No. 51571109, No. 11734006, and No. 11727808), the Fundamental Research Funds for the Central Universities (Grant No. 020414380078 and No. 020414380104). Work at CSU was supported by the U.S. National Science Foundation (EFMA1641989) and the U.S. Department of Energy, Office of Science, Basic Energy Sciences (DE-SC-0018994). H.D. acknowledges the support of China Scholarship Council (CSC) and CSU during his stay in CSU.

Conflict of Interest

The authors declare no conflict of interest.

Keywords

magnetic insulators, magneto-electric coupling, pure spin currents

Received: September 24, 2018
Revised: January 14, 2019
Published online: February 6, 2019

[1] G. A. Prinz, *Science* **1998**, *282*, 1660.
[2] H. Ohno, D. Chiba, F. Matsukura, T. Omiya, E. Abe, T. Dietl, Y. Ohno, K. Ohtani, *Nature* **2000**, *408*, 944.
[3] Y. H. Chu, L. W. Martin, M. B. Holcomb, M. Gajek, S. J. Han, Q. He, N. Balke, C. H. Yang, D. Lee, W. Hu, Q. Zhan, P. L. Yang, A. Fraile-Rodríguez, A. Scholl, S. X. Wang, R. Ramesh, *Nat. Mater.* **2008**, *7*, 478.
[4] N. A. Hill, *J. Phys. Chem. B* **2000**, *104*, 6694.
[5] W. Eerenstein, N. D. Mathur, J. F. Scott, *Nature* **2000**, *442*, 759.
[6] J. M. Hu, Z. Li, L. Q. Chen, C. W. Nan, *Nat. Commun.* **2011**, *2*, 553.
[7] M. Liu, J. Lou, S. D. Li, N. X. Sun, *Adv. Funct. Mater.* **2011**, *21*, 2593.
[8] J. Ma, J. M. Hu, Z. Li, C. W. Nan, *Adv. Mater.* **2011**, *23*, 1062.
[9] J. M. Hu, C. W. Nan, *Phys. Rev. B.* **2009**, *80*, 224416.
[10] J. M. Hu, C. W. Nan, L. Q. Chen, *Phys. Rev. B.* **2011**, *83*, 134408.
[11] Y. Wang, W. W. Lin, D. R. Qu, Q. L. Ma, Y. Zhang, Y. F. Li, S. M. Yang, C. L. Chien, *Phys. Rev. Appl.* **2018**, *10*, 014004.
[12] S. Zhang, Y. G. Zhao, P. S. Li, J. J. Yang, S. Rizwan, J. X. Zhang, J. Seidel, T. L. Qu, Y. J. Yang, Z. L. Luo, Q. He, T. Zou, Q. P. Chen, J. W. Wang, L. F. Yang, Y. Sun, Y. Z. Wu, X. Xiao, X. F. Jin, J. Huang, C. Gao, X. F. Han, R. Ramesh, *Phys. Rev. Lett.* **2012**, *108*, 137203.
[13] M. Liu, B. M. Howe, L. Grazulis, K. Mahalingam, T. X. Nan, N. X. Sun, G. J. Brown, *Adv. Mater.* **2013**, *25*, 4886.
[14] S. Murakami, N. Nagaosa, S. C. Zhang, *Science* **2003**, *301*, 1348.
[15] S. A. Wolf, D. D. Awschalom, R. A. Buhrman, J. M. Daughton, S. von Molnár, M. L. Roukes, A. Y. Chtchelkanova, D. M. Treger, *Science* **2001**, *294*, 1488.
[16] K. L. Wang, H. Lee, F. Ebrahimi, P. K. Amiri, presented at *IEEE Int. Symp. on Circuits and Systems (ISCAS)*, Montreal, QC, Canada, May **2016**.
[17] T. Schneider, A. A. Serga, B. Leven, B. Hillebrands, R. L. Stamps, M. P. Kostylev, *Appl. Phys. Lett.* **2008**, *92*, 022505.
[18] R. Lavrijsen, J. H. Lee, A. Fernández-Pacheco, D. Petit, R. Mansell, R. P. Cowburn, *Nature* **2013**, *493*, 647.
[19] A. V. Chumak, A. A. Serga, B. Hillebrands, *Nat. Commun.* **2014**, *5*, 4700.
[20] V. G. Harris, *IEEE Trans. Magn.* **2012**, *48*, 1075.
[21] A. V. Chumak, V. I. Vasyuchka, A. A. Serga, B. Hillebrands, *Nat. Phys.* **2015**, *11*, 453.
[22] B. Heinrich, C. Burrowes, E. Montoya, B. Kardasz, E. Girt, Y. Y. Song, Y. Y. Sun, M. Z. Wu, *Phys. Rev. Lett.* **2011**, *107*, 066604.
[23] Y. Y. Sun, H. C. Chang, M. Kabatek, Y. Y. Song, Z. H. Wang, M. Jantz, W. Schneider, M. Z. Wu, *Phys. Rev. Lett.* **2013**, *111*, 106601.
[24] H. L. Wang, C. H. Du, P. C. Hammel, F. Y. Yang, *Phys. Rev. Lett.* **2014**, *113*, 097202.
[25] S. Y. Huang, X. Fan, D. Qu, Y. P. Chen, W. G. Wang, J. Wu, T. Y. Chen, J. Q. Xiao, C. L. Chien, *Phys. Rev. Lett.* **2012**, *109*, 107204.
[26] B. F. Miao, S. Y. Huang, D. Qu, C. L. Chien, *Phys. Rev. Lett.* **2013**, *111*, 066602.
[27] D. Houssameddine, U. Ebels, B. Delaët, B. Rodmacq, I. Firastrau, F. Ponthenier, M. Brunet, C. Thirion, J. P. Michel, L. Prejbeanu-Buda, M. C. Cyrille, O. Redon, B. Dieny, *Nat. Mater.* **2007**, *6*, 447.
[28] H. C. Chang, P. Li, W. Zhang, T. Liu, A. Hoffmann, L. J. Deng, M. Z. Wu, *IEEE Magn. Lett.* **2014**, *5*, 6700104.
[29] Y. K. Fetisov, G. Srinivasan, *Appl. Phys. Lett.* **2006**, *88*, 143503.
[30] M. I. Bichurin, R. V. Petrov, V. M. Petrov, *Appl. Phys. Lett.* **2013**, *103*, 092902.
[31] C. Thiele, K. Dörr, O. Bilani, J. Rödel, L. Schultz, *Phys. Rev. B* **2007**, *75*, 054408.
[32] C. Zhou, G. Dunzhu, J. L. Yao, C. J. Jiang, *J. Alloys Compd.* **2017**, *710*, 680.
[33] M. Belmeguenai, F. Zighem, Y. Roussigné, S.-M. Chérif, P. Moch, K. Westerholt, G. Woltersdorf, G. Bayreuther, *Phys. Rev. B* **2009**, *79*, 024419.
[34] X. Tao, Q. Liu, B. Miao, R. Yu, Z. Feng, L. Sun, B. You, J. Du, K. Chen, S. F. Zhang, L. Zhang, Z. Yuan, D. Wu, H. F. Ding, *Sci. Adv.* **2018**, *4*, eaat1670.
[35] J. Sinova, S. O. Valenzuela, J. Wunderlich, C. H. Back, T. Jungwirth, *Rev. Mod. Phys.* **2015**, *87*, 1213.
[36] Z. Feng, J. Hu, L. Sun, B. You, D. Wu, J. Du, W. Zhang, A. Hu, Y. Yang, D. M. Tang, B. S. Zhang, H. F. Ding, *Phys. Rev. B* **2012**, *85*, 214423.
[37] L. H. Bai, Z. Feng, P. Hyde, H. F. Ding, C. M. Hu, *Appl. Phys. Lett.* **2013**, *102*, 242402.
[38] J. Y. Lian, Y. Chen, Z. Liu, M. K. Zhu, G. S. Wang, W. B. Zhang, X. L. Dong, *Ceram. Int.* **2017**, *43*, 7477.
[39] S. P. Pati, M. Al-Mahdawi, Y. Shiokawa, M. Sahashi, Y. Endo, *IEEE Trans. Magn.* **2017**, *53*, 11.
[40] M. Balinskiy, S. Ojha, H. Chiang, M. Ranjbar, C. A. Ross, A. Khitun, *J. Appl. Phys.* **2017**, *122*, 123904.
[41] Y. Tserkovnyak, A. Brataas, G. E. W. Bauer, *Phys. Rev. B* **2002**, *66*, 224403.
[42] Y. Shiomi, E. Saitoh, *Phys. Rev. Lett.* **2014**, *113*, 266602.
[43] K. Ando, S. Takahashi, J. Ieda, H. Kurebayashi, T. Trypiniotis, C. H. W. Barnes, S. Maekawa, E. Saitoh, *Nat. Mater.* **2011**, *10*, 655.
[44] M. Obstbaum, M. Härtinger, H. G. Bauer, T. Meier, F. Swientek, C. H. Back, G. Woltersdorf, *Phys. Rev. B* **2014**, *89*, 060407.
[45] M. Weiler, M. Althammer, M. Schreier, J. Lotze, M. Pernpeintner, S. Meyer, H. Huebl, R. Gross, A. Kamra, J. Xiao, Y. T. Chen, H. J. Jiao, G. E. W. Bauer, S. T. B. Goennenwein, *Phys. Rev. Lett.* **2013**, *111*, 176601.

